A THEORETICAL ANALYSIS AND EXPERIMENTAL STUDY OF A COUPLED SCREW-PNEUMATIC CONVEYOR FOR CHOPPED CORNSTALKS

Wulantuya[1], Nanding Li[1], Hongbo Wang[1*], Zhipeng Fan[1], Chunguang Wang[1], Lin Qing[1]

[1*]Corresponding author. College of Mechanical and Electrical Engineering, Inner Mongolia Agricultural University/Hohhot, China. E-mail: wanghb@imau.edu.cn | ORCID ID: https://orcid.org/0000-0001-7420-213X

ABSTRACT

Various problems are encountered during the screw feeding process of chopped cornstalk. Therefore, it is important to deeply analyze and understand the relationship between conditions and productivity of screw conveyors. This study reveals the influence of air velocity, pitch, rotational speed, and feeding rate on productivity, power consumption, specific power consumption and pressure of material for a coupled screw-pneumatic conveyor. Through a theoretical analysis, a mathematical model is established that simultaneously considers the compression characteristics of the material, material pressure from the change in pitch and centrifugal force of the screw axis, productivity of the coupled screw-pneumatic conveyor, power consumption and specific power consumption. Then, experiments are conducted to investigate the influence of the structural and working parameters of the conveyor on its performance. Finally, the correctness of the theoretical calculation is verified through a comparison with experimental results. The results of the theoretical analysis are in good agreement with the experimental results, and the relative deviations fall within 10%, 13%, 14% and 11% for the productivity, energy consumption, specific consumption and material pressure of the conveyor, respectively. With increasing airflow speed, pitch, rotational speed and feeding volume, the power consumption increases, and the other parameters have their own trends.

INTRODUCTION

Cornstalk is a renewable, ecologically friendly and widely accessible biomass resource (Long et al., 2009; Angeles et al., 2017). Cornstalk processing includes crushing, cutting and chopping. The chopping process breaks the cornstalk, including hard shells and stem nodes, into a soft, filamentous and fluffy material that is nutritious and quite suitable for digestible forage (Chu et al., 2016; Zhang & Xu, 2016; Song et al., 2017; Ma, 2018).

Conveying is one of the important parts of the cornstalk processing procedure. The most common types of conveyors for cornstalks are the pneumatic conveyor, screw conveyor, tape conveyor, board conveyor, bucket type and chain plate conveyor (Wu et al., 2013; Tian et al., 2014; Wu et al., 2017; Tian et al., 2018). Among them, the screw conveyor is widely used in the processing of cornstalk

because it is compact and airtight, its assembly is flexible, and its feed is adjustable. However, its transportation performance is unstable due to the characteristics of cornstalk, such as light density, high viscosity and poor fluidity (Wulantuya et al., 2019a). To date, the study of screw conveyors for fibrous agricultural materials has mainly focused on equipment for harvesting and processing (Kaplan et al., 2012; Jiang et al., 2013; Feng et al., 2015; Nachenius et al., 2015a and Nachenius et al., 2015b; Chamberlin et al., 2018). Our team previously investigated the screw conveying process of chopped cornstalk and found that the biomass material underwent overall screw-type motion under the joint effects of below-normal thrust and tangential friction of the screw blades and axial and circumferential friction of the screw shaft and interior casing (Wulantuya et al., 2015, 2016 and 2019a). The chopped cornstalk was constantly squeezed

during transportation. Because of its increasingly growing density, the biomass accumulated in the space between the screw shaft and case and thus generated a radial frictional force on the screw shaft, which resulted in significant wear of both the shaft and casing. Consequently, a series of problems, such as decreased productivity, increased power consumption and even jamming, occurred.

The screw flow conveyor combines flat and eddy flows, in which axial flat flow pushes the biomass material forward along the axis, determining the transportation speed, while eddy flow blows and suspends the material, thus decreasing accumulation (Ouyang et al., 2017).

In agricultural engineering, it is common to use a screw flow conveyor for the transportation of granular materials, although its application to fibrous materials is seldom seen. The Chinese Patent Office released several patents for coupled screw-pneumatic devices, but no relevant experiments or products have been reported (Liu & Luo, 2014; Liu et al., 2014; Hao et al., 2016; Wang et al., 2016).

Based on the analysis of screw conveyor characteristics and the principle of screw flow transportation, this study combined the two elements of screw flow and pneumatic coupling and produced an airflow where the screw angle of the blades produced a coupled screw-pneumatic effect in the screw groove (Wulantuya et al., 2019b, 2020 and 2021). Therefore, a theoretical analysis of the coupled screw-pneumatic conveying process with respect to the non-plug flow theory of solid transfer and fluid dynamics was conducted, and a transport model considering the compressibility and mechanical properties of the material was established accordingly. This study also tried to establish a new mathematical model that could reflect the material pressure in the groove, productivity of the screw-pneumatic device, power consumption and specific power consumption to investigate the factors and the way they influenced the performance of the device. An effective method was proposed for transporting chopped cornstalk, and this model could further serve as a reference for design of conveyors for other biomass materials.

THEORETICAL ANALYSIS OF COUPLED SCREW-PNEUM-ATIC TRANSPORT

Basic Hypotheses

This research was based on the following hypotheses:

(1) During the conveying process, the material of the chopped cornstalk was regarded as a compressible moving continuum with changeable density.

(2) A micro-scale unit was taken near the screw blade, and inside it, there was absolute contact among the material with no relative sliding. The density of the micro-scale unit was a function of pressure, and the direction of density change was only along the direction of material transport.

(3) The friction coefficients between the micro-scale unit and screw blades, central axis and casing were subject to changes in material density and moisture content.

(4) The density, axial stress (compression) and normal stress of the material micro-scale unit changed only in the direction of material transport.

(5) The curvature of the screw blades and the gap between the screw blade and casing were not considered in this study.

Velocity Analysis

The velocity analysis of the material micro-scale unit in the screw groove is shown in Figure 1 below.
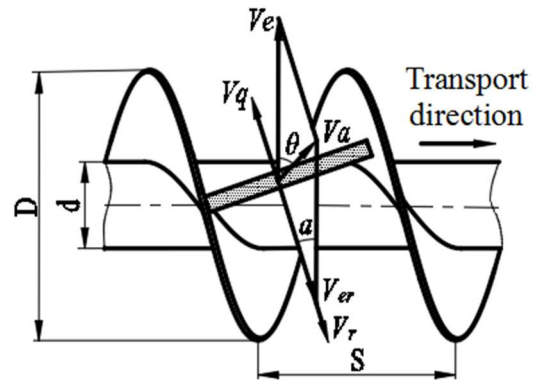
FIGURE 1. Diagram of velocity analysis.

$$V_{er} = V_r - V_q = \frac{V_e \sin\theta}{\sin(\alpha+\theta)} = \frac{\pi r n \, si}{30 \sin(\alpha+\theta)} \qquad (1)$$

$$V_e = \frac{\pi r n}{30} \qquad (2)$$

$$V_a = \frac{v_e \sin\alpha}{\sin(\alpha+\theta)} = \frac{\pi r n \sin\alpha}{\sin(\alpha+\theta)} \qquad (3)$$

Where:

V_{er} (m/s) is the equivalent relative velocity of the micro-scale unit;

V_r (m/s) is the relative velocity of the micro-scale unit under no airflow;

V_q (m/s) is the airflow velocity;

V_e (m/s) is the convected velocity of the micro-scale unit;

θ (°) is the traction angle;

α (°) is the screw angle of the screw blades;

r (mm) is the screw blade radius where the micro-scale unit is located;

n (r/min) is the rotational speed of the screw axis,

V_a (m/s) is the absolute velocity of the micro-scale unit.

Continuity Equation

During the conveying process, there was contact, compression and deformation among the chopped cornstalk. The space of the disperse system was continuously squeezed so that it could be assumed that the material density was correspondingly increasing, as shown in Figure 2.
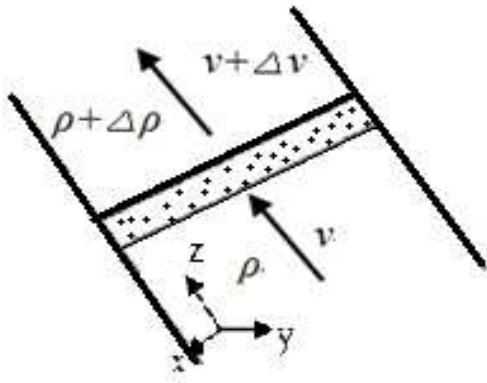
FIGURE 2. Schematic diagram of the analysis of the motion of the material.

It was assumed that a micro-scale unit was taken along the conveying direction in the screw groove. Then, $\rho v S dh$ represented the mass of flow-in the material at time dt, and $\left(\rho v + \frac{\partial(\rho v)}{\partial z} dz\right) S dh$ represented the mass of material that flowed out. $\frac{\partial \rho}{\partial t} S dh dz$ was the mass accumulation within time dt along the z-direction, according to the law of conservation of mass,

$$\rho v S dh - \left(\rho v + \frac{\partial(\rho v)}{\partial z} dz\right) S dh = \frac{\partial \rho}{\partial t} S dh dz \qquad (4)$$

which was further simplified:

$$\frac{\partial \rho}{\partial t} + \rho \frac{\partial v}{\partial z} + v \frac{\partial \rho}{\partial z} = 0 \qquad (5)$$

Where:

ρ (kg/m³) is the material density;

dh (m) is the height of the micro-scale unit;

v (m/s) is the speed of the micro-scale unit;

S (m) is the pitch of the screw blades;

dz (m) is the distance along the screw groove,

t (s) is time.

Equation of Material Motion

A material micro-scale unit was taken near the screw blade, and its force analysis was as follows, as shown in Figure 3.
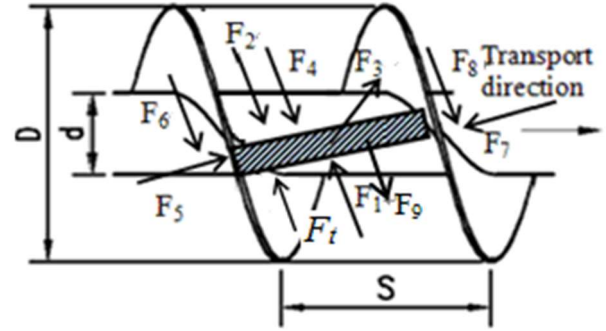
FIGURE 3. Force analysis diagram of the micro-scale unit of material.

The micro-scale unit was subject to several forces in the coupled screw-pneumatic device: thrust from the material behind $F_1 = PSdh$, frontal resistance from the material ahead $F_2 = \left(P + \frac{\partial P}{\partial z} dz\right) S dh$, friction force of the casing surface $F_3 = f_a(PSdz + \rho dz S dh a_n)$, friction force of the material $F_4 = f_c PSdz$, normal pressure on the front surface of screw blade $F_5 = Pdhdz + F_d$ and its friction force $F_6 = f_b(Pdhdz + F_d)$, normal pressure on the back side of a screw blade $F_7 = Pdhdz$ and its friction force $F_8 = f_b Pdhdz$, friction force of the material below $F_9 = f_c PSdz$, and air flow force $F_t = PSdh$. a_n is the normal acceleration of the material and $a_n = \frac{V_{er}^2}{r}(\sin \alpha \cot \theta)^2$. Then, the equation of motion of the micro-scale unit along the direction of the screw groove was:

$$F_1 + F_t - F_2 + F_3 \cos(\alpha + \theta) - F_4 + F_5 \sin \alpha - F_6 - F_7 \sin \alpha - F_8 - F_9 = \rho S dh dz \frac{dv}{dt} \qquad (6)$$

Expressions for F_d、 F_5、 and F_6 were obtained from the force analysis in the x-direction, and then by substituting $F_1 \sim F_9$ and F_d into [eq. (6)]:

$$PSdh + P_t Sdh - (P + \frac{\partial P}{\partial z} dz)Sdh + f_a(PSdz + \rho Sa_n dzdh) \cos(\alpha + \theta) - f_c PSdz + Pdhdz \sin \alpha + f_a(PSdz +$$

$$\rho Sa_n dzdh) \sin(\alpha + \theta) \tan \alpha - f_b Pdhdz - \frac{f_a f_b (PSdz + \rho Sa_n dzdh) \sin(\alpha+\theta)}{\cos \alpha} - Pdhdz \sin \alpha - f_b Pdhdz - f_c PSdz = \rho S dh dz \frac{dv}{dt} \qquad (7)$$

By simplifying the above expression:

$$\frac{\partial P}{\partial z} + PK_f + \rho \left(v \frac{\partial v}{\partial z} + \frac{\partial v}{\partial t} + K_b v^2\right) = 0 \qquad (8)$$

Where:

$$K_f = \frac{f_a}{dh}\left[\frac{2f_c}{f_a} - cos(\alpha + \theta) - sin(\alpha + \theta)tan\,\alpha + \frac{f_b}{f_a}\frac{2dh}{S} + \frac{f_b\,sin(\alpha+\theta)}{cos\,\alpha} - \frac{dh}{f_aP}\cdot\frac{P_t}{dz}\right] \qquad (9)$$

$$K_b = \frac{f_a}{r}(sin\,\alpha\,cot\,\theta)^2\left[\frac{f_b\,sin(\alpha+\theta)}{cos} - sin(\alpha + \theta)tan\,\alpha - cos(\alpha + \theta)\right] \qquad (10)$$

and:

f_a is the friction coefficient of the material and casing;

f_b is the friction coefficient of the material and screw blade and screw axis,

f_c is the internal friction coefficient of the material, and P_t is the air flow pressure in Pa.

Solution of the Mathematical Model

$\bar{P}$, $\bar{\rho}$, $\bar{v}$, and $\bar{t}$ are assumed to be the eigenvectors of pressure, density, velocity and time, respectively. L (m) is the length of the screw conveyor in the axial direction. v_0 (m/s) is the inlet velocity of the material in the steady state and $v_0 = 2\pi rn\,cos\,\alpha$. P_0 (Pa) is the initial pressure. Assuming that $P = \bar{P}(1 + P^*)$, $\rho = \bar{\rho}(1 + \rho^*)$, $v = \bar{v}(1 + v^*)$, $t = \bar{t}t^*$, and $z = Lz^*$,

then, the corresponding dimensionless boundary is:

$$\begin{cases} v^*|_{z^*=0} = \frac{v(z,\,t)|_{z=0}}{\bar{v}} - 1 = v_0^*(t) = v_0^* \\ v^*|_{t^*=0} = 0 \end{cases} \qquad (11)$$

$$\begin{cases} P^*|_{z^*=0} = \frac{P(z,\,t)|_{z=0}}{\bar{P}} - 1 = P_0^*(t) = P_0^* \\ P^*|_{t^*=0} = 0 \end{cases} \qquad (12)$$

Using the dimensionless method, linearization method, and Laplace transform, the continuity equation and motion equation led to:

$$P = P_0 e^{-\frac{\gamma_1 z}{L}} \qquad (13)$$

$$V = v_0 - \frac{C_0 v_0 (\rho_m - \bar{\rho})(\bar{P} - P_0)}{\bar{\rho}}(e^{-\gamma_1 z} - 1) \qquad (14)$$

Herein, $\gamma_1 = \frac{\rho_0(P_0 L K_f + L K_b \rho_m v_0^2)}{P_0[\rho_0 - \rho_m v_0^2 C_0(\rho_m - \rho_0)]}$ is the initial density of the material ρ_0 (kg/m³). The pressure of the Material is:

$$P(Z) = \int_0^Z \int_0^H P dh dz = \int_0^Z \int_0^H P_0 e^{-\frac{\gamma_1 z}{L}} dz dh \qquad (15)$$

Theoretical Model of Productivity

The volume productivity Q_v (m³/min) was calculated according to the equations below:

$$Q_v = AV_x = 2\pi rn\frac{tan\,\alpha\,tan\,\theta}{tan(\alpha + \theta)}\left[\frac{\pi(D^2 - d^2)}{4} - \frac{eH}{s\iota\tilde{n}\,\alpha}\right] \qquad (16)$$

$$A = \frac{\pi(D^2 - d^2)}{4} - \frac{eH}{s\iota\tilde{n}\,\alpha} \qquad (17)$$

$$V_x = 2\pi rn\frac{tan\,\alpha\,tan\,\theta}{tan\,\alpha + tan\,\theta} \qquad (18)$$

Where:

V_x (m/s) is the component of absolute velocity V_a (m/s) in the axial direction;

A (m²) is the material cross-sectional area perpendicular to the axis;

D (m) is the outside diameter of the screw blades;

d (m) is the diameter of the central axis;

H (m) is the height of the screw blades;

e (m) is the thickness of the screw blades,

$\bar{\alpha}$ (°) is the average helix angle.

The productivity of the screw-pneumatic coupled conveyor is:

$$Q_g = Q_v\rho = 2\pi rn\rho\frac{tan\,\alpha\,tan\,\theta}{tan(\alpha + \theta)}\left[\frac{\pi(D^2 - d^2)}{4} - \frac{eH}{s\iota\tilde{n}\,\alpha}\right] \qquad (19)$$

Theoretical model of power consumption

The total power consumption of the coupled screw-pneumatic conveyor included E_0, E_1, E_2, E_3 and E_4. Among them, E_0 is the power consumption of effects related to windings, extrusion, and friction. E_1 is the power consumption by friction between the material and casing surface. E_2 is the power consumption by friction between the material and the pressure surface as well as the back sides of the screw blades. E_3 is the power consumption by friction between the material and the central axis. E_4 is the power consumption of the pump.

$$E_1 = \int_0^Z \int_0^H F_3 V_a \, dh \, dz \qquad (20)$$

$$E_2 = \int_0^Z \int_0^H (F_6 + F_8 - F_t) V_{er} \, dh \, dz \qquad (21)$$

$$E_3 = \int_0^Z \int_0^H F_c V_{er} \, dh \, dz \qquad (22)$$

The total power consumption of the coupled screw-pneumatic conveyor is:

$$E = k(E_1 + E_2 + E_3) + E_4 \qquad (23)$$

Productivity and power consumption are principal indices for conveying performance for chopped cornstalk. There is actually a certain connection between productivity and power consumption, and thus that they should be considered simultaneously to evaluate the conveying performance of the coupled screw-pneumatic coupled conveyor for chopped cornstalk. Therefore, the concept of specific power consumption was used in this study. It is the power consumption per unit mass of material conveyed. This is a critical index for the conveying performance of the screw-pneumatic coupled conveyor. The formula is as follows:

$$\eta = \frac{E}{Q_g} \qquad (24)$$

MATERIAL AND METHODS

The material tested in this study was cornstalk rubbed by a 9R-60 chopping machine (Manufactured by the Inner Mongolia Agricultural University Machinery Factory, Hohhot, China). With a length less than 100 mm and an average moisture content of 38% (Wang & Han, 2019; Li et al., 2022), the chopped cornstalk conformed to the requirements of NY/T509-2002 Plant Stalk Chopping Machinery, Agricultural Standard of China.

Test Equipment
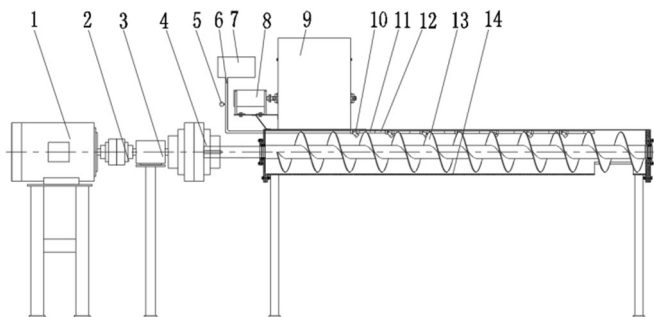
1-Motor, 2-Couplings, 3-Measuring instrument of speed and torque, 4-Couplings, 5-Pressure gauge, 6-High-pressure explosion-proof air pipe, 7-Air compressor, 8-Single-phase direct current speed regulating motor, 9-Feeder, 10-Y-shaped nozzle, 11-Straight pipe, 12-Bent pipe, 13-Screw axis, 14-Casing.

FIGURE 4. Structure of the test unit of the coupled screw-pneumatic conveyor.

Figure 4 shows the structure of the coupled screw-pneumatic conveyor. It mainly consisted of two parts: a screw conveyor system and a pneumatic conveyor system. The screw conveyor system included a motor, flexible coupling, torque speed meter, feeder, screw axis and casing. Auxiliary to the screw conveyor system, the pneumatic conveyor system included a Y-shaped nozzle, nozzle base, air compressor, air pipe and pressure gauge. Some primary parameters were as follows: 2500 mm conveying length, 250 mm outside diameter of the screw blade, 60 mm diameter of the screw axis, adjustable pitch, 260 mm×400 mm feeder inlet, 5 ~ 8 mm gap between the screw blade and casing, and adjustable rotational speed for the screw axis and feeder. Furthermore, a testing system for axial thrust and power consumption was designed for the device.

The nozzle unit mainly consisted of a nozzle holder and a nozzle, which are shown in Figure 5. A Y-shape nozzle holder was chosen with an adjustable spray direction and a fixed nozzle.
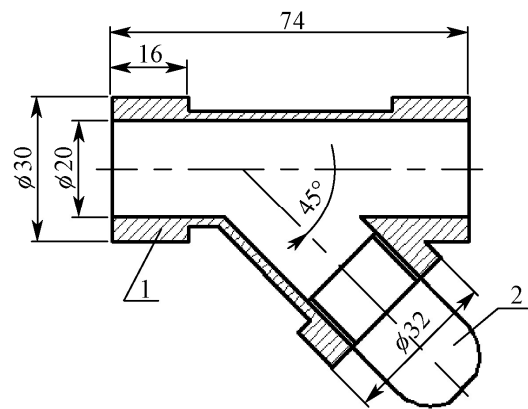
1-Y-shaped nozzle holder, 2-Nozzle.

FIGURE 5. Structure diagram of the nozzle device unit.

To reduce the repeat area and the empty area of the airflow barrier in the spiral groove, one nozzle was installed every 335 mm over the entire conveying length, for a total of seven. In the middle of each of the two nozzles, a section of straight pipe and a bent pipe were installed. The straight pipe was a polypropylene random (Abbreviation is PPR) pipe with an ultimate working pressure of 1.6 MPa and a radius of 10 mm. A 15° pipe was chosen to change the position of the airflow in the radial direction to stagger the airflow barrier of the adjacent two nozzles and prevent cancellation of the airflows.

Design of Test System

It was difficult to measure the pressure inside the rubbed corn stalk when it was being transported. To approximate the pressure of the material, round force sensors were deployed on the screw-pneumatic device to monitor axial thrust under different working conditions.

Figure 5 shows a block diagram of the testing system for axial thrust and power consumption. It mainly consisted of a frequency converter, a three-phase induction motor, a round force sensor (LDCZL-FK type, 1000N/0.01N, LD, Ltd., Beijing, China), a digital display controller (LDCHB, LD, Ltd., Beijing, China), a torque speed sensor (JN388 type, SanJing, Ltd., Beijing, China) and a torque speed meter (JN388 type, SanJing, Ltd., Beijing, China) as well as a computer.

```
┌─────────────────────────────────────────┐
│      CNT800-4T0075G type transducer      │
└─────────────────────────────────────────┘
                    │
                    ▼
┌─────────────────────────────────────────┐
│  Y10012 type three-phase asynchronous motor │
└─────────────────────────────────────────┘
                    │
                    ▼
┌─────────────────────────────────────────┐
│       JN388 type torque speed sensor     │
└─────────────────────────────────────────┘
                    │
                    ▼
┌─────────────────────────────────────────┐
│              Screw conveyor              │
└─────────────────────────────────────────┘
                    │
                    ▼
┌─────────────────────────────────────────┐
│      LDCZL-FK type round force sensor    │
└─────────────────────────────────────────┘
```
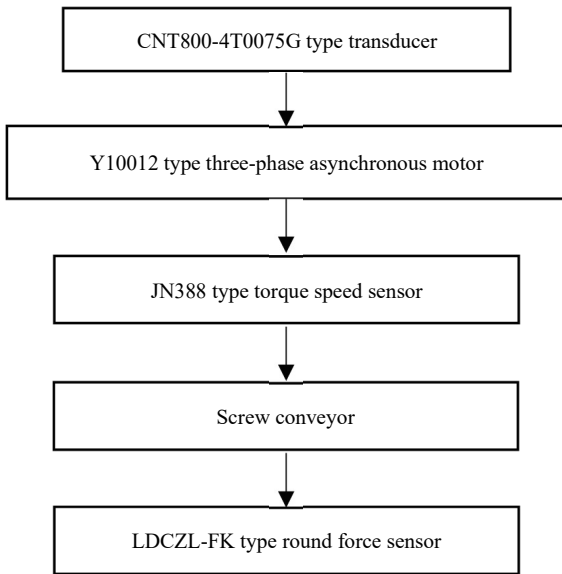
FIGURE 6. Block diagram of the testing system.

In the testing system, a JN388-type torque speed sensor was used to monitor the power consumption of the device in real time, and a JN388-type torque speed meter was used for data collection and output. LDCZL-FK-type round force sensors were deployed to monitor axial thrust at the thrust bearings, and an LDCHB-type digital display controller was used for data collection and output.

Choice of level of factors

According to a previous study, the screw-pneumatic conveyor worked well when the pitch of the screw blade was set in the range of 250～375 mm, the feeding rate was 10～70 kg/min and the rotational speed for the screw axis was 40～120 r/min. Therefore, in this study, the levels of factors were controlled within the ranges shown in Table 1.

TABLE 1. Levels of test factors.

Levels	Factors			
	Pitch S/mm	Rotational speed n/(r·min^{-1})	Feeding quantity Φ/(kg·min^{-1})	Airflow velocity v/(m·s^{-1})
1	250	40	30	10
2	300	60	50	20
3	335	80	70	30
4	355	100		40
5	375	120		50

RESULTS AND DISCUSSION

Substituting the parameters for the coupled screw-pneumatic conveyor and material into eqs (15), (19), (23) and (24), the values of performance parameters were calculated and compared with actual test values to analyze the influence of airflow, pitch, rotational speed and feeding quantity on material pressure, productivity, power consumption and specific power consumption.

Influence of air flow on conveyor performance

As shown in Figure 7, when the pitch was 335 mm, the rotational speed of the screw axis was 100 r/min and the feeding rate was 70 kg/min, and there were increases in the airflow velocity, productivity (Figure 7(a)) and power consumption (Figure 7(b)) of the coupled screw-pneumatic conveyor. The velocity analysis indicated that an increase in airflow velocity decreased the equivalent velocity of the material relative to the screw blades; thus, circular motion weakened and productivity increased. Meanwhile, a screw flow was generated along the screw groove as a result of the coupled screw-pneumatic force. The axial flat flow pushed the chopped cornstalk along the screw axis and sped its movement in the screw groove to reduce axial hysteresis and axial thrust (Figure 7(d)). Eddy flow blew the chopped cornstalk upward and made it fluffy to prevent the material from compressing or jamming and effectively increased productivity.
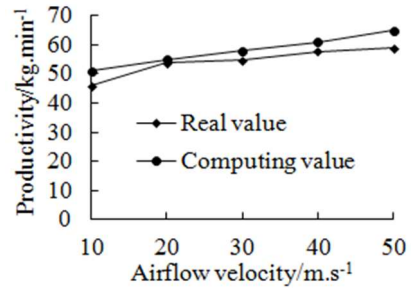
(a) Relationship between airflow velocity and productivity.
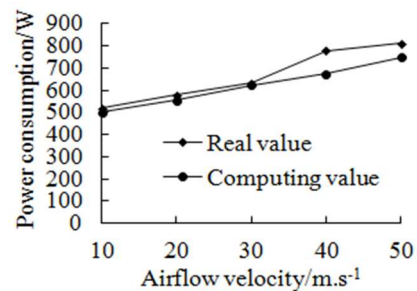
(b) Relationship between airflow velocity and power consumption.
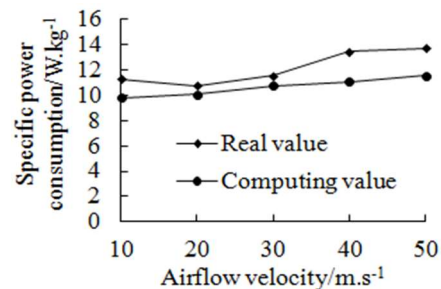
(c) Relationship between airflow velocity and specific power consumption.
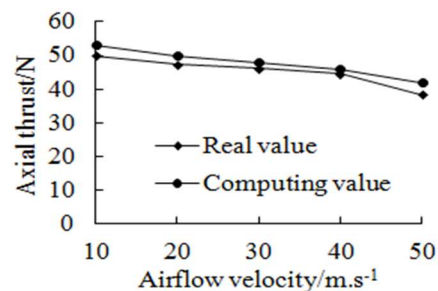
(d) Relationship between airflow velocity and axial thrust.

FIGURE 7. Conveying performance at different airflow velocities.

Formula (23) revealed that the screw blades, device casing and central axis could exert friction forces on the material so that a small screw-pneumatic force had little influence on the material movement but increased the total power consumption of the device. When the airflow velocity reached a certain value, the screw-pneumatic force overcame friction and thus generated a screw flow along the screw groove, resulting in the specific power consumption first decreasing and increasing (as in Figure 7(c)). When the airflow velocity was 20 m/s, the specific power consumption reached the minimum value, 10.78 W/kg, which was significantly 8.3% smaller than that for no airflow.

By comparison between the measured value and calculated value, as shown in Figure 7, the theoretical curve and test curve changed in the same pattern with a relative error within 10%.

As shown in Figure 7(a), the theoretical value of the productivity was greater than the measured value. Although the productivity model neglected the gap between the screw blades and casing as well as the influence of material movement along the direction of blade height direction, due to the material characteristics, the actual feeding rate was different from the predetermined feeding rate while feeding, and there was axial hysteresis.

For power consumption, as shown in Figure 7(b), the measured value was greater than the theoretical value. The main reason was that the theoretical calculation did not consider the power losses from friction, stirring, twining and accumulation of chopped cornstalk in the screw groove.

However, for the axial thrust, as shown in Figure 7(d), the theoretical value was greater than the measured value for the following two reasons: 1. The thrust model was established, and a force analysis was conducted based on the hypothesis that the material was a moving continuum that has no interior space, which increased the theoretical value. 2. When pushed forward, the material exerted counter-forces on the screw blades, casing and central axis, specifically an axial thrust at the thrust bearing and a certain pressure inside the screw groove. However, only the axial thrust was finally considered and compared to the theoretical value, and thus the theoretical value was larger than the measured value.

Pitch influence on conveyor performance

In Figure 8, productivity (Figure 8(a)) and power consumption (Figure 8(b)) both increased with increasing pitch, while specific power consumption first fell and then rose (Figure 8(c)), and axial thrust only decreased (Figure 8(d)).

(b) Relationship between pitch and power consumption.
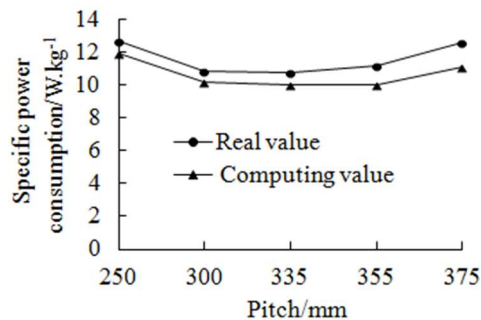
(c) Relationship between pitch and specific power consumption.
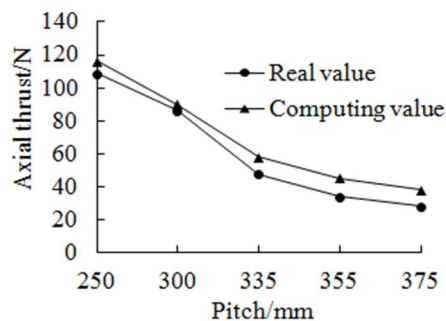
(d) Relationship between pitch and axial thrust.

FIGURE 8. Conveying performance at different pitches

This was because a greater pitch value enlarged the space between adjacent blades and thus lessened material compression in the screw groove, resulting in improved transport of material and reduced axial thrust, which propelled the axial movement of the material and hence raised the productivity. However, a considerably larger pitch increased the kinetic energy of the material and the power consumption; thus, the specific power consumption first diminished and then increased.

In the comparison between the measured values and calculated values, as displayed in Figure 8, the theoretical curve and test curve changed with the same trend with relative error within 13%. For productivity and axial thrust, the theoretical values were greater than their measured values, while for power consumption, its theoretical value was smaller than its measured value. Thus, the theoretical ratio of power consumption to productivity-specific power consumption was smaller than its measured value.

(a) Relationship between pitch and productivity.

Influence of rotational speed on conveyor performance

Figure 9 shows that along with the increase in rotational speed, the productivity increased and then decreased (Figure 9(a)), while the specific power consumption, in contrast, first decreased and then increased again (Figure 9(c)). Both the power consumption (Figure 9(b)) and the axial thrust (Figure 9(d)) increased.

The theoretical analysis in Part 2 revealed that increasing rotational speed resulted in blades propelling more material forward and hence increasing the conveying capacity. However, when the rotational speed exceeded a critical value, more material engaged in circular movement so that the conveying efficiency and productivity decreased.

According to the theory of contact mechanics (Tang et al., 2012) and the characteristics of rubbed cornstalks, there are four contact states between the material and blades: separation, adhesion, absolute sliding and partial sliding. A change in the rotational speed of the screw axis led to a change in the relative tangential speed between the material and blades, and thus the friction coefficient and consequently the contact state of the contact area as well as the axial thrust changed.

According to the Stribeck friction model, there is a certain nonlinear relationship between the friction coefficient of two objects in contact and the relative tangential speed. With growing rotational speed of the screw axis, the friction coefficient first decreased and then increased (Thomsen & Fidlin, 2003; Li et al., 2012). During the period of decreasing coefficient of friction, there was relative sliding between the material and blades, and the friction between them was mainly responsible for the power consumption. During the period of increasing coefficient of friction, the friction between the material and blades was so large that either material tightly adhered to the blades or there was only partial sliding between them.
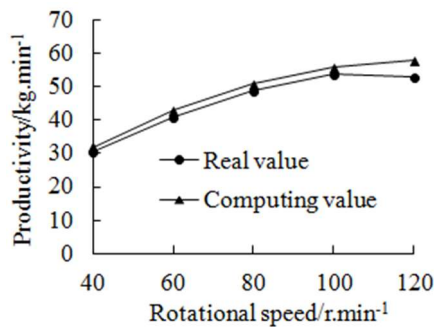
(a) Relationship between rotational speed and productivity
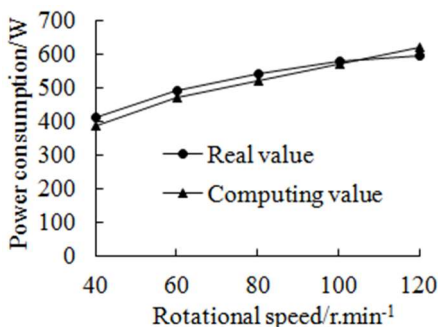
(b) Relationship between rotational speed and power consumption.
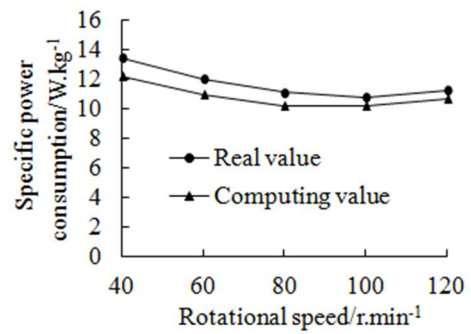
(c) Relationship between rotational speed and specific power consumption.
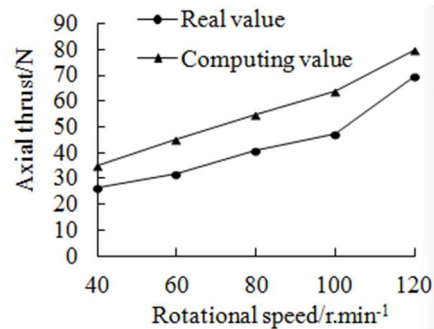
(d) Relationship between rotational speed and axial thrust.

FIGURE 9. Conveying performance at different rotational speeds.

At this point, the force between the material undergoing circular movement and material undergoing axial movement was mainly responsible for power consumption. That is, power consumption increased with rotational speed.

In a comparison between the measured values and calculated values, as displayed in Figure 9, the theoretical curve and test curve changed in the same pattern with a relative error within 14%. For productivity (Figure 9(a)) and axial thrust (Figure 9(d)), the theoretical values were greater than the measured values, while for power consumption (Figure 9(b)), the theoretical value was smaller than the measured value. As a result, the theoretical value of specific power consumption being smaller than its measured value (Figure 9(c)).

Influence of feeding rate on conveyor performance

Figure 10 shows that productivity, power consumption, specific power consumption and axial thrust all increased with increasing feeding rate. This was mainly because a growing feeding rate increased the quantity of material in the screw groove and hence raised the productivity. Additionally, the blades propelled the material forward and compressed it so that the axial thrust and overall power consumption increased.

In a comparison between the measured value and calculated value, as displayed in Figure 10, the theoretical curve and test curve changed with the same trend with a relative error within 12%. For productivity (Figure 10(a)) and axial thrust (Figure 10(d)), the theoretical values were greater than the measured values, while for power consumption (Figure 10(b)), the theoretical value was smaller than the measured value. As a result, the theoretical value of specific power consumption was smaller than its measured value (Figure 10(c)).
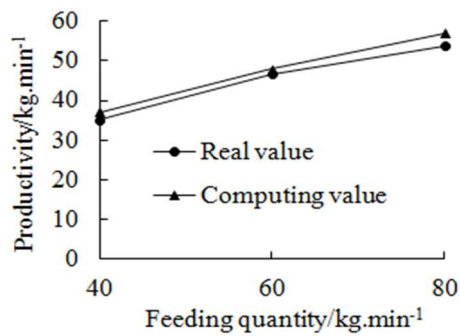
(a) Relationship between feeding quantity and productivity.
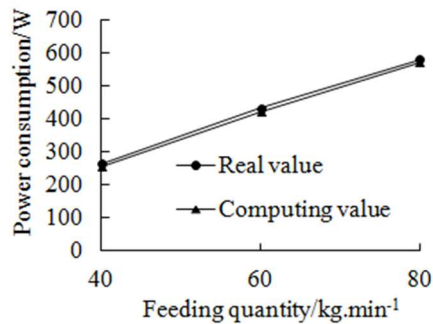
(b) Relationship between feeding quantity and power consumption.
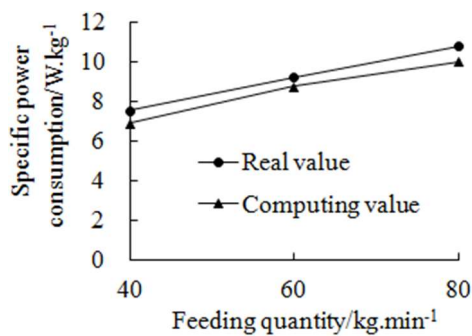
(c) Relationship between feeding quantity and specific power consumption.
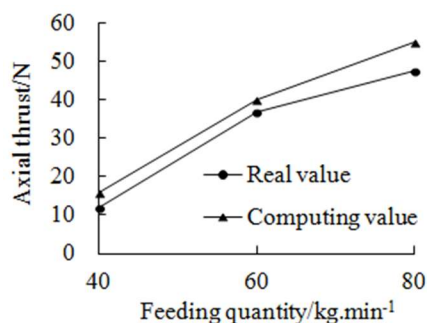
(d) Relationship between feeding quantity and axial thrust.

FIGURE 10. Conveying performance for different feeding quantities.

CONCLUSIONS

According to the non-plug flow theory of solid transfer and fluid dynamics, this study investigated the coupled screw-pneumatic conveying process for chopped cornstalk and established a mathematical model that simultaneously considered the compression characteristics of the material, changes in the pitch and centrifugal force of the screw axis, and pressure of the material in the screw groove as well as productivity, power consumption and specific power consumption of the coupled screw-pneumatic conveyor.

Experiments were conducted to determine the influence of the structural and working parameters of the coupled screw-pneumatic conveyor on the material pressure, productivity, power consumption and specific power consumption. The results revealed that within the range of 10～50 m/s, both the productivity and power consumption of the coupled screw-pneumatic conveyor increased with increasing airflow velocity. In contrast, the specific power consumption first decreased and then increased while the material pressure decreased.

When the airflow velocity was 20 m/s, the minimum specific power consumption was 10.78 W/kg, which was 8.3% smaller than without airflow. When the pitch changed from 250 ～ 375 mm, both the productivity and power consumption increased. When the rotational speed of the screw axis was in the range of 40～120 r/min, the productivity first increased and then decreased, while the power consumption only increased, with increasing rotational speed. Meanwhile, the specific power consumption first decreased and then increased, and the material pressure fell. In the range of 10～70 kg/min feeding rate, the productivity, power consumption, specific power consumption and pressure all increased with increasing feeding rate.

The experimental test results verified the computational results for productivity, power consumption, specific power consumption and material pressure with relative errors less than 10%, 13%, 14% and 12%, respectively.

ACKNOWLEDGEMENTS

REFERENCES

Angeles GM, Conesa JA, Dolores GM (2017) Characterization and production of fuel briquettes made from biomass and plastic wastes. Energies 10(7): 1-12. https://doi.org/10.3390/en10070850

Chamberlin C, Carter D, Jacobson A (2018) Measuring residence time distributions of wood chips in a screw conveyor reactor. Fuel Processing Technology 178: 271-282. https://doi.org/10.1016/j.fuproc.2018.06.005

Chu TS, Yang ZL, Han LJ (2016) Analysis on satisfied degree and advantage degree of agricultural crop straw feed utilization in China. Transactions of the Chinese Society of Agricultural Engineering (Transactions of the CSAE) 32(22): 1-9. https://doi.org/10.11975/j.issn.1002-6819.2016.22.001

Feng L, Li TS, Xu KH (2015) Design of screw conveyor device for biomass crushing and molding machine. Forest Engineering 31(3): 101-105. https://doi.org/10.16270/j.cnki.slgc.2015.03.025

Hao M, Li QW, Wang JX (2016) Pneumatic and screw conveyors: 201620575164.1[P]. 2016-6-13.

Jiang EC, Su XL, Wang MF, Xiong LM, Zhao C, Xu XW (2013) Design of variable pitch spiral conveyor for biomass continual pyrolysis reactor. Transactions of the Chinese Society for Agricultural Machinery 44(2): 121-124. https://doi.org/10.6041/j.issn.1000-1298.2013.02.023

Kaplan Ozgur, Celik Cenk (2012) Woodchip drying in a screw conveyor dryer. Journal of Renewable and Sustainable Energy 4(6):1-12. https://doi.org/10.1063/1.4766890

Li QS, Zhu Y, Tan HL, Zhang JQ (2012) Improvement of 3D contact problem FEA under variable friction condition. Journal of Mechanical Engineering 23(16): 1929-1933. https://doi.org/10.3969/j.issn.1004-132X.2012.16.009

Li XF, Wang YS, Sun Y, Sun CY (2022) Present situation of corn straw resources in China and research progress in feed conversion. Feed Research 45(18): 129-132. https://doi.org/10.13557/j.cnki.issn1002-2813.2022.18.026

Liu SM, Luo ZW (2014) A pneumatic screw conveyor: 201420630587.X[P]. 2014-10-29.

Liu ZM, Zhong YY, Li CH (2014) A pneumatic auxiliary screw conveyor: 201420873476.1[P]. 2014-12-31.

Long JC, Li X, Lu JH (2009) Renewable energy from agro-residues in China: Solid biofuels and biomass briquetting technology. Renewable and Sustainable Energy Reviews 13: 2689-2695. https://doi.org/10.1016/j.rser.2009.06.025

Ma CL (2018) Improved design of 9RS-2 Straw Kneading Machine. Dissertation, Gansu Agricultural University of China.

Nachenius RW, Wardt TA, Ronsse F, Prins W (2015a) Residence time distributions of Coarse biomass particles in a screw conveyor reactor. Fuel Processing Technology 130:87-95. https://doi.org/10.1016/j.fuproc.2014.09.039

Nachenius RW, Wardt TA, Ronsse F, Prins W (2015b) Torre faction of pine in a bench-scale screw conveyor reactor. Biomass & Bioenergy 79:96-104. https://doi.org/10.1016/j.biombioe.2015.03.027

Ouyang LG, Zhao YJ, Peng Q, Wei QR (2017) Conveying efficiency optimization of stirred tank spiral flow field based on pneumatic conveyance. Engineering Machinery 48(12): 22-29.

Song ZW, Wang J, Zhu XL, Zhong ZN, Pan Y, Qiao YY (2017) Present research status and prospects of the comprehensive utilization of straw resources. Journal of Anhui Agricultural Sciences 45(7): 64-66: 162. https://doi.org/10.13989/j.cnki.0517-6611.2017.07.025

Tang JY, Zhou W, Chen SY (2012) Analysis of frictional contact problem for curved surface coupling with velocity using finite element algorithm. Journal of Chongqing University 35(6): 43-47.

Thomsen JJ, Fidlin A (2003) Analytical approximations for stick-slip vibration amplitudes. International Journal of Non-Linear Mechanics 38(3): 389-403. https://doi.org/10.1016/S0020-7462(01)00073-7

Tian Y, Lin J, Li BF (2018) Design and test of conveying device of pneumatic straw deep burying and returning machine. Transactions of the Chinese Society for Agricultural Machinery 12: 36-44. https://doi.org/10.6041/j.issn.1000-1298.2018.12.005

Tian YS, Fu CG, Wu YL, Zhao LX, Yao ZL, Meng HB (2014) Analysis of influencing factors on crop stalk's mass transfer of belt conveyor. Transactions of the Chinese Society of Agricultural Engineering (Transactions of the CSAE) 30(14): 219-226. https://doi.org/10.3969/j.issn.1002-6819.2014.14.028

Wang DX, Liu YY, Qiao SJ (2016) A spiral pneumatic composite conveying mechanism: 201620340854.9[P]. 2016-4-22.

Wang YQ, Han XP (2019) Research advance on pathway of corn straw for feed. Feed Research 42(07): 117-120. https://doi.org/10.13557/j.cnki.issn1002-2813.2019.07.032

Wu F, Xu HB, Gu FW, Chen YQ, Shi LL, Hu ZC (2017) Improvement of straw transport device for straw-smashing back-throwing type multi-function no-tillage planter. Transactions of the Chinese Society of Agricultural Engineering (Transactions of the CSAE) 33(24): 18-26. https://doi.org/10.11975/j.issn.1002-6819.2017.24.003

Wu YL, Hou SL, Zhao LX, Tian YS, Meng HB (2013) Development and prospect of straw conveyor technology and equipment. Journal of Agricultural Mechanization Research (9): 11-16. https://doi.org/10.13427/j.cnki.njyi.2013.09.034

Wulantuya, Qing L, Wang CG (2019a) Design of screw-pneumatic coupling conveying device for crushed corn straw. Transactions of the Chinese Society of Agricultural Engineering (Transactions of the CSAE) 32(6): 29-38. https://doi.org/10.11975/j.issn.1002-6819.2019.06.004

Wulantuya, Wang CG, Qi SH, Meng JG, Wang JL (2015) Test and analysis of performance of screw conveyor for rubbing and breaking corn straw. Transactions of the Chinese Society of Agricultural Engineering (Transactions of the CSAE) 31(21): 51-59. https://doi.org/10.11975/j.issn.1002-6819.2015.21.007

Wulantuya, Wang CG, Qi SH, Wang XR, Wang HC, Wang JL (2016) Theoretical model analysis and test of screw conveyor for rubbing and breaking corn straw. Transactions of the Chinese Society of Agricultural Engineering (Transactions of the CSAE) 32(22): 18-26. https://doi.org/10.11975/j.issn.1002-6819.2016.22.003

Wulantuya, Wang CG, Zhao FC, Wang XR (2019b) Experiment and optimization of screw conveyor parameters for rubbing and breaking corn straw. Journal of China Agricultural University 24(2): 115-122. https://doi.org/10.11841/j.issn.1007-4333.2019.02.13

Wulantuya, Wang HB, Wang CG, Qinglin (2020) Theoretical Analysis and experimental study on the process of conveying agricultural fiber materials by screw conveyors. Engenharia Agrícola 40 (05): 589-594. https://doi.org/10.1590/1809-4430-eng.agric.v40n5p589-594/2020

Wulantuya, Wuyuntana, Wang HB, Guo WB, Wang CG, Qinglin (2021) Mechanical characteristics of the rubbed maize straw during screw conveying. INMATEH Agricultural Engineering 64(2): 109-118. https://doi.org/10.35633/inmateh-64-10

Zhang SX, Xu Q (2016) Study of 9ZS-4 forage grass crushing machine and its design. Machine Building & Automation 45(5): 147-149. https://doi.org/10.19344/j.cnki.issn1671-5276.2016.05.042